

## Optical properties of strain-free AlN nanowires grown by molecular beam epitaxy on Si substrates

Q. Wang,<sup>1</sup> S. Zhao,<sup>1</sup> A. T. Connie,<sup>1</sup> I. Shih,<sup>1</sup> Z. Mi,<sup>1,a)</sup> T. Gonzalez,<sup>2</sup> M. P. Andrews,<sup>2</sup> X. Z. Du,<sup>3</sup> J. Y. Lin,<sup>3</sup> and H. X. Jiang<sup>3</sup>

<sup>1</sup>Department of Electrical and Computer Engineering, McGill University, 3480 University Street, Montreal, Quebec H3A 0E9, Canada

<sup>2</sup>Department of Chemistry, McGill University, 801 Sherbrooke St West, Montreal, Quebec H3A 0B8, Canada

<sup>3</sup>Department of Electrical and Computer Engineering, Texas Tech University, Lubbock, Texas 79409, USA

(Received 22 March 2014; accepted 22 May 2014; published online 4 June 2014)

The optical properties of catalyst-free AlN nanowires grown on Si substrates by molecular beam epitaxy were investigated. Such nanowires are nearly free of strain, with strong free exciton emission measured at room temperature. The photoluminescence intensity is significantly enhanced, compared to previously reported AlN epilayer. Moreover, the presence of phonon replicas with an energy separation of  $\sim 100$  meV was identified to be associated with the surface-optical phonon rather than the commonly reported longitudinal-optical phonon, which is further supported by the micro-Raman scattering experiments. © 2014 AIP Publishing LLC. [<http://dx.doi.org/10.1063/1.4881558>]

AlN and Al-rich AlGa<sub>N</sub> alloy have been considered as the materials of choice for deep ultraviolet (DUV) optoelectronic devices, including light emitting diodes (LEDs), laser diodes, and photodetectors, due to their wide direct band-gap.<sup>1,2</sup> These materials also exhibit many unique properties, such as extreme thermal and chemical stability, high mechanical strength, hardness, and corrosion resistance, which make them suitable for applications in harsh environments. Similar to other III-nitride semiconductors, AlN epilayers have been commonly grown on highly lattice-mismatched substrates such as sapphire or SiC, and the resulting large densities of dislocations ( $\sim 10^7$ – $10^{10}$  cm<sup>-2</sup>) and other structural defects severely limit the device performance.<sup>3</sup> Moreover, the extraction efficiency of DUV emitters is extremely low due to the strong polarization of emitted light with  $E \parallel c$ .<sup>4</sup> To enhance the external quantum efficiency, various strategies, including micro-LEDs and photonic crystals, have been employed to extract the light that propagates transversely ( $E \perp c$ ) in DUV emitters.<sup>5</sup>

These critical issues may be potentially addressed by utilizing low-dimensional structures such as nanowires for the following reasons. First, the dislocation/defect density can be drastically reduced in nanowires due to the completely removed epitaxial relationship between the nanowires and the underlying substrate,<sup>6</sup> as well as the highly effective lateral strain relaxation.<sup>7</sup> Second, the intrinsically larger light extraction efficiency of nanowires may further enhance the external quantum efficiency, especially for DUV emitters.<sup>8</sup> In addition, another major bottleneck for DUV optoelectronic devices, i.e., the extreme difficulty in impurity doping, can be potentially addressed by the reduced formation energy for substitutional doping in the near surface region of nanowires, rendering enhanced surface doping and conductivity in nanowire devices.<sup>9</sup> In this regard, tremendous efforts have been devoted to synthesizing/growing

AlN nanowires via different techniques, including chemical vapour deposition, direct current arc discharge method, and molecular beam epitaxy (MBE).<sup>10–14</sup> To date, however, such AlN nanowires generally exhibit extremely poor structural and optical properties, *with no reports on the band-edge optical emission at room temperature*. In addition, a detailed understanding of many other important properties of AlN nanowires, including the strain distribution and the influence of surface on the optical emission, has remained elusive.

In this Letter, we have investigated the MBE growth and characterization of nearly strain-free AlN nanowires on GaN nanowire templates on Si (111) substrates. Such nanowires exhibit strong free exciton (FX) emission at 6.03 eV at low temperature. The photoluminescence (PL) spectral linewidth is  $\sim 21$  meV, which is significantly smaller than that ( $\sim 33$  meV) measured in high quality AlN epilayers, suggesting drastically improved crystalline quality. A strong and pure PL spectrum was also measured at room temperature. Moreover, the presence of phonon replicas in the AlN nanowires shows an energy separation of  $\sim 100$  meV, which is identified to be associated with the surface-optical (SO) phonons rather than the commonly measured longitudinal-optical (LO) phonons. This observation is further supported by the micro-Raman scattering experiments.

Catalyst-free AlN nanowires were grown on Si (111) substrates using a Veeco Gen II MBE system under nitrogen-rich conditions. Prior to the growth of AlN nanowires, GaN nanowire arrays were first grown, which serve as a template to promote the formation of AlN nanowires. This is schematically shown in Fig. 1(a). Compared with the direct nucleation of AlN on Si or dielectric layer SiO<sub>x</sub>,<sup>13</sup> the utilization of the GaN nanowire template can provide a better control of the AlN nanowire size, density, and quality and is fully compatible with processes for achieving DUV devices on a Si-platform.<sup>15</sup> The growth conditions included a plasma power of 350 W, a nitrogen flow rate of 1 sccm, an Al flux of  $6 \times 10^{-8}$  Torr, and a growth temperature of 858 °C for the AlN nanowires. Structural properties of the AlN

<sup>a)</sup>Author to whom correspondence should be addressed. Electronic mail: [zetian.mi@mcgill.ca](mailto:zetian.mi@mcgill.ca).

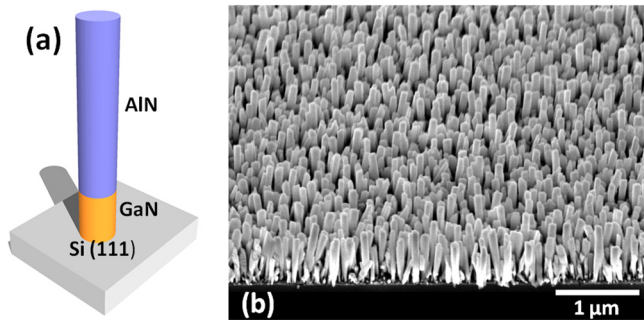


FIG. 1. (a) Schematic diagram showing AlN nanowires grown on GaN nanowire template on Si substrate. (b) Typical bird's-eye-view SEM image of AlN nanowires taken with a 45-deg angle.

nanowires were examined using a high-resolution scanning electron microscope (SEM) with an acceleration voltage of 5 kV. A representative SEM image of the AlN nanowires is presented in Fig. 1(b). It can be seen that the AlN nanowires are vertically aligned on Si substrate. The diameter and the density of the AlN nanowires are estimated to be  $\sim 100$  nm and  $1 \times 10^{10} \text{ cm}^{-2}$ , respectively. Transmission electron microscope (TEM) studies further indicate that such nanowires are nearly defect-free.

Detailed PL emission characteristics were studied subsequently. For PL measurements, a frequency-quadrupled Ti-sapphire laser (with lasing wavelength of 197 nm, 76 MHz repetition rate, 100 fs pulse width, and average optical power of about 1 mW) was used as an excitation source. The laser beam was focused onto the nanowire sample by a lens. The PL signal was collected and dispersed by a monochromator (1.3 m), and then detected by a microchannel-plate photo-multiplier tube together with a single photon-counting system.<sup>4</sup>

Figure 2(a) shows the PL spectrum of the AlN nanowires measured at low temperature (10 K). For comparison, the PL spectrum of high quality AlN epilayers grown on a sapphire substrate is also shown in Fig. 2(b) measured side-by-side under identical conditions. The thickness of the AlN epilayer is  $\sim 1 \mu\text{m}$ , which is comparable to the height of AlN nanowires. Since the quantum confinement effect in nanowires with diameters  $\sim 100$  nm is negligible, the excitonic transitions in nanowires and epilayers can be compared directly. Shown in Fig. 2(b), the FX emission ( $n=0$  line) in AlN epilayers was observed at  $\sim 6.06$  eV with its phonon replicas at 5.95 eV ( $n=1$  line) and 5.84 eV ( $n=2$  line), which is similar to our previous reports.<sup>16</sup> For the presented AlN nanowires, however, the FX emission was measured at  $\sim 6.03$  eV ( $n=0$  line) with its phonon replicas at 5.93 eV ( $n=1$  line) and 5.83 eV ( $n=2$  line). The difference in the phonon replica energy ( $\sim 10$  meV) will be discussed later on. It is of interest to note that the FX peak energy ( $\sim 6.03$  eV) in AlN nanowires is almost identical to that of AlN bulk crystal and AlN epilayers,<sup>16–18</sup> This finding indicates that the AlN nanowires are virtually free of strain, which is in direct contrast to the FX emission peak energy ( $\sim 6.06$  eV) measured in compressively strained AlN epilayers grown on a sapphire substrate. Such a strain reduction in AlN nanowires is further confirmed by micro-Raman scattering experiments, as will be discussed later on. In addition, a much narrower

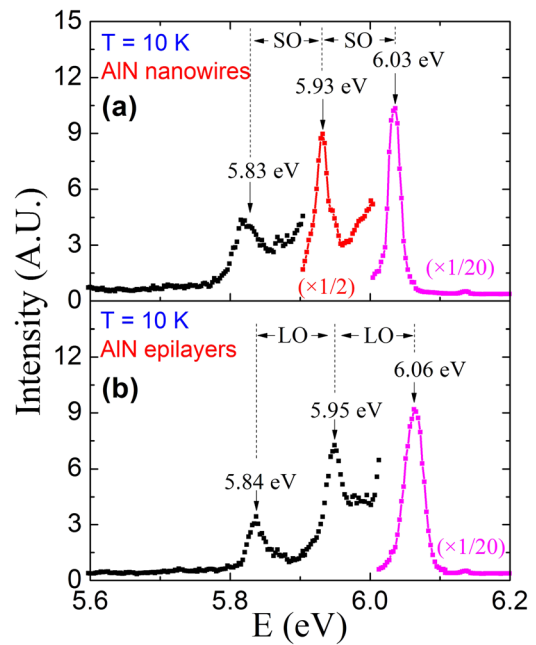


FIG. 2. (a) PL spectrum of AlN nanowires measured at 10 K with the main peak at  $\sim 6.03$  eV and SO-phonon replicas with  $\sim 100$  meV energy separation. (b) PL spectrum of AlN epilayer grown on sapphire measured at 10 K with the main peak at  $\sim 6.06$  eV and LO-phonon replicas with  $\sim 110$  meV separation.

full-width-at-half-maximum (FWHM) of the FX emission peak (21 meV) was measured in AlN nanowires compared to that measured from AlN epilayer (33 meV). This suggests much improved crystalline quality for the AlN nanowires.

The dramatically improved crystalline quality of AlN nanowires is further evidenced from Fig. 3, where an FX emission peak at  $\sim 5.96$  eV was measured at room temperature. In this case, the peak intensity is more than two times stronger than that measured from the AlN epilayer. The enhanced optical emission cannot be attributed only to the improved crystalline quality in the AlN nanowire bulk region, but also suggests that surface defects/states of AlN nanowires have a relatively minor impact on the excitonic

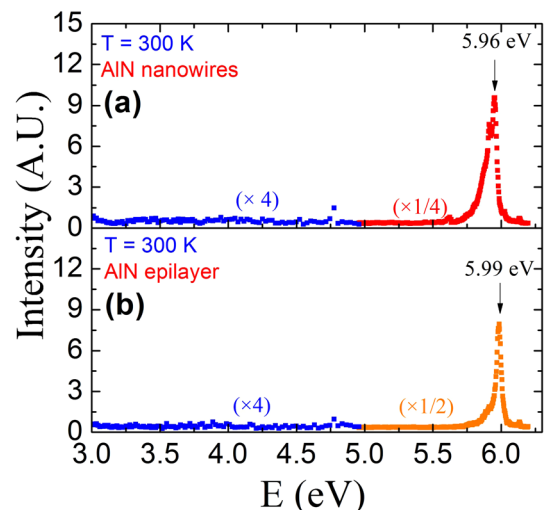


FIG. 3. (a) PL spectrum of AlN nanowires measured at 300 K with the main peak at  $\sim 5.96$  eV. (b) AlN epilayer grown on sapphire measured at 300 K with the main peak at  $\sim 5.99$  eV.

recombination dynamics. We attribute this mainly to the large exciton binding energy ( $\sim 60$  meV) and very small Bohr radius of the exciton ( $\sim 1.2$  nm) in AlN resulting from the large effective mass of carriers.<sup>19</sup> Such ultra-stable excitons dominate the recombination process even at room temperature and hence prevent carriers from being captured by surface defects/states in nanowires, thereby effectively suppressing surface related non-radiative recombination.

Now let us focus on the phonon replicas in AlN nanowires. It is noticed that the energy separation between the phonon replicas is only  $\sim 100$  meV (Fig. 2(a)), which is about 10 meV smaller than that of the typical LO-phonon replicas in AlN epilayers, illustrated in Fig. 2(b). Such a large energy difference suggests that the origin of phonon replicas in AlN nanowires is probably associated with other types of phonon modes rather than the typical LO-phonon.<sup>20</sup> Generally speaking, the unique configuration of polar semiconductor nanostructures (e.g., nanowires), including the large aspect ratio and/or small transversal dimension, could lead to the appearance of vibrational phonon modes that are related to the oscillation of surface atoms.<sup>21–23</sup> Such SO-phonons are sensitive to the morphology, size, and density of nanowires and are also a function of the dielectric constant of the environment.<sup>23</sup> Based on Loudon's uniaxial crystal model and within the framework of the dielectric continuum model, it has been estimated that the SO-phonon energy in AlN nanowires can be varied from 84 meV to 110 meV.<sup>24</sup> Therefore, the phonon replicas in the presented AlN nanowires are likely due to the interaction between SO-phonon and electrons via the Fröhlich electron-phonon coupling.

In order to further support this conclusion, micro-Raman experiments were performed at room temperature with a 488 nm Argon ion laser through a  $100\times$  objective. The focused laser spot size was  $\sim 1$   $\mu\text{m}$ . Figure 4 shows a typical Raman spectrum of AlN nanowires taken with unpolarized light in the backscattering geometry, i.e.,  $z(\dots)\bar{z}$  configuration. It is seen that a strong Si signal, which is peaked at  $520\text{ cm}^{-1}$  (not shown) dominates, and an AlN  $E_2^H$  mode is observed at  $\sim 656\text{ cm}^{-1}$ . The peak position of the  $E_2^H$  mode

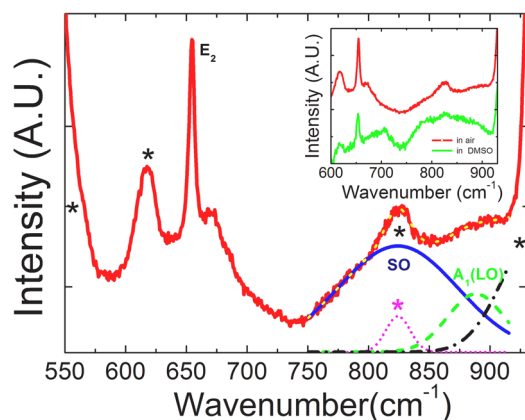


FIG. 4. Typical room temperature micro-Raman spectrum of AlN nanowires (spectrum is scaled out focusing on AlN modes, and Si/SiO<sub>2</sub> modes are pointed out with “\*”). Gaussian curve fitting (from  $750\text{ cm}^{-1}$  to  $915\text{ cm}^{-1}$ ) showing the SO-phonon mode (blue solid curve), Si mode (pink dotted curve), A<sub>1</sub>(LO) mode (green short dashed curve), background signal from SiO<sub>2</sub> (black dash-dotted curve). Inset: micro-Raman spectra measured in air and DMSO, respectively.

has been widely used to evaluate the strain conditions in III-nitride semiconductors, due to its high sensitivity to the biaxial strain in the  $c$ -plane. In this study, a negligible shift is observed in the  $E_2^H$  mode (less than  $1\text{ cm}^{-1}$ ), compared with that measured in AlN bulk crystal, confirming that the AlN nanowires are nearly free of strain as discussed above.<sup>25</sup>

Moreover, the typical A<sub>1</sub>(LO) phonons at  $\sim 890\text{ cm}^{-1}$  cannot be clearly distinguished in the measured spectrum, partly due to the presence of a strong asymmetric broad band at its lower energy side. By using standard Gaussian curve fitting (from  $750\text{ cm}^{-1}$  to  $915\text{ cm}^{-1}$ ) shown in Fig. 4, it has been found that such a broad band is composed of a sharp mode (pink dotted curve) from Si substrate and another broad mode (blue solid curve), which is attributed to the SO-phonon mode with the peak at  $\sim 825\text{ cm}^{-1}$ . Also in this fitting, the green dashed curve is assigned to the A<sub>1</sub>(LO) mode and black dash-dotted curve is due to the strong background signal from SiO<sub>2</sub>. The observed SO-phonon mode was also reported in GaN nanowires, AlN nanotips and GaN/AlN core-shell nanowires with frequency ranging between the TO and LO phonon mode.<sup>23,26,27</sup> Moreover, the Raman spectrum of AlN nanowires was also recorded in dimethyl sulfoxide (DMSO) ( $\epsilon_m = 45$ ) as shown in the inset of Fig. 4. It can be observed that immersing nanowires in materials with a high dielectric constant leads to an obvious shape change and redshift of the asymmetric broad band. This result provides further evidence for the presence of a strong SO-phonon mode in the measured spectrum. Importantly, the energy of the presented SO-phonon mode is estimated to be  $\sim 102$  meV, nearly identical to the energy separation between the phonon replicas in AlN nanowires shown in Fig. 2(a). This result confirms that the origin of phonon replicas measured in AlN nanowires is due to the interaction between electron and SO-phonon rather than LO-phonon. The presence of a strong SO-phonon mode could be related to the oxidation of AlN nanowire surfaces.<sup>10</sup> The formation energy analysis suggests that oxygen could be easily incorporated in AlN by substituting for nitrogen atoms.<sup>28,29</sup> In addition, negatively charged vacancies  $V_{\text{Al}}^{3-}$  in AlN were found to be energetically favourable and thus could bind to positively charged substitutional oxygen forming defect complexes on the surfaces of nanowires.<sup>12,29,30</sup>

The coupling strength between phonon and exciton can be evaluated by using the Huang–Rhys (H-R) factor, i.e.,  $S$ -factor, based on the equation  $I_n = I_0 (S^n/n!)$ .<sup>31</sup> Here,  $n = 0, 1, 2, 3, \dots$ , represent the number of LO-phonons involved,  $I_n$  is the emission intensity of the  $n$ th phonon replica and  $I_0$  is the intensity of the main emission line. Accordingly, based on Figs. 2(a) and 2(b), the  $S$ -factors are determined to be 0.15 and 0.11 for AlN nanowires and epilayers, respectively. Both  $S$ -factors are much larger than those for GaN epilayers (0.007) due to the smaller Bohr radii of excitons in AlN and other reasons.<sup>32</sup> In this study, a larger  $S$ -factor, i.e., a stronger phonon-exciton coupling in nanowires, could also originate from the significantly improved material quality, since the emission intensity of phonon replicas can be significantly reduced by the scattering of impurities and defects.<sup>31</sup> Additionally, it is worth highlighting that the frequency of the SO-phonon in nanowires can be tuned by changing the morphology, wire density, and the dielectric constant of the



environment.<sup>23</sup> Therefore, the SO-phonon assisted excitonic transitions could also be engineered accordingly. This provides the possibility and a certain degree of freedom in designing phonon-assisted optoelectronic devices, which has not been previously possible for the conventional LO-phonon assisted process.

In conclusion, we have demonstrated strain-free AlN nanowires grown directly on Si substrate by the catalyst-free MBE process, which can exhibit superior optical properties, including strong PL emission and a narrower spectral line-width, compared to previously reported AlN epilayers. Moreover, the unique SO-phonon replica with an energy separation  $\sim 100$  meV was observed in PL spectra of AlN nanowires. These observations are also supported by micro-Raman scattering measurements.

This work was supported by the Natural Sciences and Engineering Research Council of Canada and the Fonds de recherche sur la nature et les technologies. The authors wish to thank Dr. Omid Salehzadeh at McGill University and Prof. Li Zhang at Panyu Polytechnic in China for useful discussions with micro-Raman and theoretical simulation, respectively. The PL measurement is supported by the Department of Energy (Grant #FG02-09ER46552), USA. H. X. Jiang and J. Y. Lin are grateful to the AT&T Foundation for the support of Ed Whitacre and Linda Whitacre Endowed chairs.

<sup>1</sup>Y. Taniyasu, M. Kasu, and T. Makimoto, *Nature* **441**, 325 (2006).

<sup>2</sup>J. Li, Z. Y. Fan, R. Dahal, M. L. Nakarmi, J. Y. Lin, and H. X. Jiang, *Appl. Phys. Lett.* **89**, 213510 (2006).

<sup>3</sup>B. N. Pantha, R. Dahal, M. L. Nakarmi, N. Nepal, J. Li, J. Y. Lin, H. X. Jiang, Q. S. Paduano, and D. Weyburne, *Appl. Phys. Lett.* **90**, 241101 (2007).

<sup>4</sup>K. B. Nam, J. Li, M. L. Nakarmi, J. Y. Lin, and H. X. Jiang, *Appl. Phys. Lett.* **84**, 5264 (2004).

<sup>5</sup>J. Shakya, K. H. Kim, J. Y. Lin, and H. X. Jiang, *Appl. Phys. Lett.* **85**, 142 (2004).

<sup>6</sup>S. Zhao, M. G. Kibria, Q. Wang, H. P. T. Nguyen, and Z. Mi, *Nanoscale* **5**, 5283 (2013).

<sup>7</sup>F. Glas, *Phys. Rev. B* **74**, 121302 (2006).

<sup>8</sup>A.-L. Henneghien, G. Tourbot, B. Daudin, O. Lartigue, Y. Désières, and J.-M. Gérard, *Opt. Express* **19**, 527 (2011).

<sup>9</sup>S. Zhao, S. Fatholouloumi, K. Bevan, D. Liu, M. Kibria, Q. Li, G. Wang, H. Guo, and Z. Mi, *Nano Lett.* **12**, 2877 (2012).

<sup>10</sup>Kenry, K.-T. Yong, and S. Yu, *J. Mater. Sci.* **47**, 5341 (2012).

<sup>11</sup>X. H. Ji, S. P. Lau, S. F. Yu, H. Y. Yang, T. S. Heng, A. Sedhain, J. Y. Lin, H. X. Jiang, K. S. Teng, and J. S. Chen, *Appl. Phys. Lett.* **90**, 193118 (2007).

<sup>12</sup>G. R. Yazdi, P. O. Å. Persson, D. Gogova, R. Fornari, L. Hultman, M. Syväjärvi, and R. Yakimova, *Nanotechnology* **20**, 495304 (2009).

<sup>13</sup>O. Landré, V. Fellmann, P. Jaffrennou, C. Bougerol, H. Renevier, A. Cros, and B. Daudin, *Appl. Phys. Lett.* **96**, 061912 (2010).

<sup>14</sup>J. H. He, R. S. Yang, Y. L. Chueh, L. J. Chou, L. J. Chen, and Z. L. Wang, *Adv. Mater.* **18**, 650 (2006).

<sup>15</sup>Q. Wang, H. P. T. Nguyen, K. Cui, and Z. Mi, *Appl. Phys. Lett.* **101**, 043115 (2012).

<sup>16</sup>B. N. Pantha, N. Nepal, T. M. Al Tahtamouni, M. L. Nakarmi, J. Li, J. Y. Lin, and H. X. Jiang, *Appl. Phys. Lett.* **91**, 121117 (2007).

<sup>17</sup>E. Silveira, J. A. Freitas, Jr., O. J. Glembocki, G. A. Slack, and L. J. Schowalter, *Phys. Rev. B* **71**, 041201 (2005).

<sup>18</sup>M. Feneberg, R. A. R. Leute, B. Neuschl, K. Thonke, and M. Bickermann, *Phys. Rev. B* **82**, 075208 (2010).

<sup>19</sup>K. B. Nam, J. Li, M. L. Nakarmi, J. Y. Lin, and H. X. Jiang, *Appl. Phys. Lett.* **82**, 1694 (2003).

<sup>20</sup>X. B. Zhang, T. Taliencio, S. Kolliakos, and P. Lefebvre, *J. Phys.: Condens. Matter* **13**, 7053 (2001).

<sup>21</sup>R. Gupta, Q. Xiong, G. D. Mahan, and P. C. Eklund, *Nano Lett.* **3**, 1745 (2003).

<sup>22</sup>C. Chen, M. Dutta, and M. A. Stroschio, *J. Appl. Phys.* **96**, 2049 (2004).

<sup>23</sup>R. Mata, A. Cros, K. Hestroffer, and B. Daudin, *Phys. Rev. B* **85**, 035322 (2012).

<sup>24</sup>L. Zhang, J.-j. Shi, and T. L. Tansley, *Phys. Rev. B* **71**, 245324 (2005).

<sup>25</sup>A. R. Goñi, H. Siegle, K. Syassen, C. Thomsen, and J. M. Wagner, *Phys. Rev. B* **64**, 035205 (2001).

<sup>26</sup>A. Cros, R. Mata, K. Hestroffer, and B. Daudin, *Appl. Phys. Lett.* **102**, 143109 (2013).

<sup>27</sup>S. Sahoo, S. Dhara, A. K. Arora, R. Krishnan, P. Chandramohan, and M. P. Srinivasan, *Appl. Phys. Lett.* **96**, 103113 (2010).

<sup>28</sup>T. Mattila and R. M. Nieminen, *Phys. Rev. B* **54**, 16676 (1996).

<sup>29</sup>C. G. Van de Walle and J. Neugebauer, *J. Appl. Phys.* **95**, 3851 (2004).

<sup>30</sup>R. A. Youngman and J. H. Harris, *J. Am. Ceram. Soc.* **73**, 3238 (1990).

<sup>31</sup>A. Sedhain, J. Li, J. Y. Lin, and H. X. Jiang, *Appl. Phys. Lett.* **95**, 061106 (2009).

<sup>32</sup>W. Liu, M. F. Li, S. J. Xu, U. Kazuo, and M. Koh, *Semicond. Sci. Technol.* **13**, 769 (1998).